Real-time formalism for studying the nonlinear response of "smart" materials to an electric field

J. K. Freericks
Department of Physics
Georgetown University
Washington, DC 20057
Email: freericks@physics.georgetown.edu

V. M. Turkowski
Department of Physics
Georgetown University
Washington, DC 20057
Email: turk@physics.georgetown.edu

V. Zlatić
Institute of Physics
Bijenicka c. 46, P. O. B. 304
10000 Zagreb, Croatia
Email: zlatic@ifs.hr

***Abstract*— The nonlinear response of a material to a large electric field (steady or pulsed) often determines the ultimate performance of the material for electronics applications. The formalism for understanding nonlinear effects in conventional semiconductors is well understood. The formalism is less well developed for so-called "smart" materials that are tuned to lie close to the metal-insulator transition. Here we show that the nonlinear response of a strongly correlated electronic material can be calculated with a massively parallel algorithm by discretizing a continuous matrix operator on the Kadanoff-Baym contour in real time. We benchmark the technique by examining the solutions when the field vanishes and comparing the results to exact results from an equilibrium formalism. We briefly discuss the numerical issues associated with the case of a large electric field and present results that show how the Bloch oscillations become damped as the scattering due to electron correlations increases.**

I. Introduction

THE problem of the response of materials used in electronics to large external fields is important from both a theoretical and a practical point of view. On the theoretical side, the basic ideas of nonequilibrium statistical mechanics were developed over 40 years ago [1], [2], but the formalism has not been applied to strongly correlated materials except in approximate ways. It is interesting to determine exact results for electronic systems in an external field which can be used to benchmark these approximate techniques. On the practical side, it is often the nonlinear behavior of the material or device that determines the ultimate performance within electronics. For example, the nonlinear current-voltage characteristic of a p-n junction is critical for semiconductor-based switching and digital logic, while the nonlinear current-voltage characteristic of a nonhysteretic Josephson junction allows for digital logic based on rapid single flux quantum (RSFQ) ideas [3]. A "smart" material is a material that can have its properties altered by changing an external system variable like pressure, temperature, or a gate voltage. The most common devices with tunability are currently based on semiconductors or ferroelectrics, but there is increasing interest in strongly correlated materials near the metal-insulator transition, because they might allow for more tunability than their semiconducting counterparts.

The interest in large electric fields arises as the system dimensions shrink onto the nanoscale. When a feature size is on the order of 100 nm, a potential difference of 1 V produces an electric field of $E \sim 10^7$ V/cm over the feature area. In addition, the military is interested in the robustness of devices to large pulsed fields that can arise from natural sources like lightning, or from man-made sources like those employed in electronic warfare. These high energy-density short-time pulsed fields may be difficult to filter out of a device and can cause the device to "burn out".

A "smart material" tuned to lie close to the metal-insulator transition is called a strongly correlated material. The name arises from the fact that one needs to take into account the electron-electron repulsion in determining how the material responds to external perturbations. In conventional metals, insulator, and semiconductors, it is adequate to ignore the mutual electron-electron repulsion, and treat all of the electrons as independent, moving in an average field created by the other electrons. This is the regime where band-theory holds. But as the electron-electron interactions are made stronger relative to the kinetic energy of the electrons, then the electron correlations need to be taken into account, implying that one cannot treat the other electrons in an averaged way, but one needs to take into account where the electrons are and how they move as every other electron moves. This is the regime of strong electron correlations, and as the correlations are increased, many materials will undergo a metal-insulator transition called the Mott-Hubbard transition.

The simplest model which takes into account strong electron-electron correlations is the Falicov-Kimball model [4]. This model has two kinds of electrons, itinerant electrons and localized electrons. They interact by a Coulomb repulsion when they both occupy the same unit cell of the lattice. If the number of itinerant electrons plus the number of localized electrons is equal to the number of lattice sites, then the system will undergo a metal-insulator transition as the Coulomb repulsion is increased. This model is not appropriate to describe many real materials, but its simplicity allows for many exact results to be calculated which are vitally important for benchmarking purposes.

II. Formalism

We consider the Falicov-Kimball (FK) model in the presence of an external electric field that is spatially uniform, but can be time-dependent, and can have an arbitrarily large amplitude. The FK model has two kinds of electrons: itinerant electrons with creation and annihilation operators $c_i^\dagger$ and c_i for conduction electrons at site i and localized electrons with the corre-

sponding operators $f_i^\dagger$ and f_i. The FK Hamiltonian is

$$\mathcal{H} = -\sum_{ij} t_{ij} c_i^\dagger c_j + U \sum_i c_i^\dagger c_i f_i^\dagger f_i - \mu \sum_i c_i^\dagger c_i + E_f \sum_i f_i^\dagger f_i, \tag{1}$$

where t_{ij} is the nearest-neighbor hopping matrix, U is the on-site repulsion between c and f electrons, μ is the chemical potential of the conduction electrons and E_f is the site energy for the localized electrons. In the simplest case, we ignore the spin of the electrons and assume they are spinless. In the calculations presented here, we set $\mu = U/2$, $E_f = -U/2$, so that $\langle c^\dagger c\rangle = \langle f^\dagger f\rangle = 1/2$; this case is called half filling.

The electric field $\mathbf{E}(\mathbf{r},t)$ is described by a vector potential $\mathbf{A}(\mathbf{r},t)$ in the Landau gauge where the scalar potential vanishes:

$$\mathbf{E}(\mathbf{r},t) = -\frac{1}{c}\frac{\partial \mathbf{A}(\mathbf{r},t)}{\partial t}\,. \tag{2}$$

We assume that the vector potential $\mathbf{A}(\mathbf{r},t)$ is smooth enough in space, that the magnetic field produced by $\mathbf{A}(\mathbf{r},t)$ can be neglected.

The electric field is introduced into the Hamiltonian (1) by the so-called Peierls' substitution [5], [6] where we neglect interband transitions because we are considering only a single band (the possible dipole transition from a localized electron state to a conduction electron state is also neglected; this assumption may break down if the localized particles are electrons, but it cannot break down if they are ions as in a binary alloy interpretation of the FK model):

$$t_{ij} \to t_{ij} \exp\left[-\frac{ie}{\hbar c}\int_{\mathbf{R}_i}^{\mathbf{R}_j} \mathbf{A}(\mathbf{r},t)\cdot d\mathbf{r}\right]. \tag{3}$$

The Peierls' substitution represents the effect of the line integral of the vector potential on the hopping between sites i (at position $\mathbf{R}_i$) and j (at position $\mathbf{R}_j$); in this work $t_{ij} \neq 0$ only for nearest-neighbor sites i and j.

For simplicity we shall study the case of a d-dimensional hypercubic lattice in the limit of large spatial dimensions $d \to \infty$. In this limit, the electron self-energy becomes local, which simplifies both the formalism and the numerical calculations. This approximation corresponds to the dynamical mean-field theory (DMFT) limit [7]. The simplest electric field is one that lies along the unit cell diagonal [8]:

$$\mathbf{A}(t) = A(t)(1,1,...,1). \tag{4}$$

After the Peierls' substitution, the "band-structure" in the electric field becomes

$$\epsilon_{\mathbf{k}} = -2t\sum_l \cos\left[a\left(\mathbf{k}_l - \frac{e\mathbf{A}_l(t)}{\hbar c}\right)\right], \tag{5}$$

with a the lattice spacing which we will take to be one. With our choice for the electric field along the diagonal, this becomes

$$\epsilon_{\mathbf{k}} = \cos\left(\frac{eA(t)}{\hbar c}\right)\varepsilon_{\mathbf{k}} + \sin\left(\frac{eA(t)}{\hbar c}\right)\bar{\varepsilon}_{\mathbf{k}}, \tag{6}$$

with

$$\varepsilon_{\mathbf{k}} = -\frac{t^*}{\sqrt{d}}\sum_l \cos k_l \tag{7}$$

and

$$\bar{\varepsilon}_{\mathbf{k}} = -\frac{t^*}{\sqrt{d}}\sum_l \sin k_l. \tag{8}$$

being generalized energy functions and t^* is a renormalized hopping parameter: $t = t^*/2\sqrt{d}$ in the limit $d \to \infty$ [7]; t^* will be used as our energy unit.

We find that many quantities we want to determine involve a summation over momenta of functions of ε and $\bar{\varepsilon}$. These summations can be performed more easily by determining a joint density of states for the two energies in Eqs. (7) and (8); the result in the limit of the infinite dimensions [9] becomes:

$$\rho_2(\varepsilon,\bar{\varepsilon}) = \frac{1}{\pi t^{*2}}\exp\left[-\frac{\varepsilon^2}{t^{*2}} - \frac{\bar{\epsilon}^2}{t^{*2}}\right].$$

Hence, a summation over an infinite-dimensional Brillouin zone can be re-expressed as a two-dimensional Gaussian integral.

In order to solve the many-body problem, we need to determine the electronic Green's functions in the presence of the electric field. The derivation of formulas for these Green's functions is more complicated than in the absence of a field, because there is no time-translation invariance, so the Green's functions depend on two different time arguments. Furthermore, since the system evolves in the presence of an electric field, there is no simple way to relate the quantum-mechanical state at large times to the state at small times. Hence, we evolve the system forward in time, then we de-evolve it backwards in time, in order to properly determine its complete time evolution. Since the local f-electron number is conserved, and we are not coupling the f electrons to the field, the Hamiltonian is a quadratic function of the conduction electron operators. This means the time-ordered product can be directly evaluated, and relevant functional derivatives can be taken to determine the Green's functions. The algebra is somewhat long and will be omitted here. The end result is a series of equations for the so-called local contour-ordered Green's function, which is defined with two time arguments, each one lying on the Kadanoff-Baym contour (see Fig. 1): $g^c(t,t') = -(i/\hbar)\langle \mathcal{T}_c c_i(t) c_i^\dagger(t')\rangle$, with the time-ordering taking place along the contour, the time dependence of the fermionic operators being determined by the total (time-dependent) Hamiltonian in the Heisenberg picture, and the angular brackets denoting a weighted trace over all states $\langle\mathcal{O}\rangle = \mathrm{Tr} e^{-\beta\mathcal{H}}\mathcal{O}/\mathcal{Z}$; the partition function is $\mathcal{Z} = \mathrm{Tr} e^{-\beta\mathcal{H}}$ with $\beta = 1/T$ the inverse temperature. In addition, we need to define a local self-energy $\Sigma^c(t,t')$ and an effective dynamical mean-field $\lambda^c(t,t')$ in analogy with the equilibrium case in zero electric field [10], [11]:

$$g^c(t,t') = \int d\varepsilon \int d\bar{\varepsilon}\rho_2(\varepsilon,\bar{\varepsilon})\left[g_0^{c-1}(\varepsilon,\bar{\varepsilon}) - \Sigma^c\right]^{-1}(t,t') \tag{9}$$

$$\lambda^c(t,t') = g_{imp}^{c-1}(t,t') - g^{c-1}(t,t') - \Sigma^c(t,t') \tag{10}$$

$$\begin{aligned} g^c(t,t') &= [1-w_1][g_{imp}^{c-1}[\mu] - \lambda^c]^{-1}(t,t') \\ &+ w_1[g_{imp}^{c-1}[\mu\to\mu-U] - \lambda^c]^{-1}(t,t') \end{aligned} \tag{11}$$

$$\Sigma^c(t,t') = g_{imp}^{c-1}(t,t') - g^{c-1}(t,t') - \lambda^c(t,t'), \tag{12}$$

where $g_0^c(\varepsilon, \bar{\varepsilon}, t, t')$ is the noninteracting Green's function in the presence of the electric field [8], $g_{imp}^c(t, t')$ is the impurity Green's function in zero field, which is equal to $g_0^c(\varepsilon, \bar{\varepsilon}, t, t')$ at $\varepsilon = \bar{\varepsilon} = 0$, and w_1 is the occupancy of the f-electrons $[w_1 = \langle f^\dagger f \rangle]$. The difference of this system of equations from the real-frequency case is that these objects are all continuous square matrix operators of time (defined on the Kadanoff-Baym time contour) rather than being scalar functions of frequency. The inverses are all to be interpreted as matrix inverses.

We will be interested in the so-called lesser Green's function $g^<$ and self-energy $\Sigma^<$ in this work. These functions are extracted from the contour-ordered objects by fixing the first time argument t to lie on the upper real-time piece of the Kadanoff-Baym contour and the second time argument t' to lie on the lower real-time piece of the Kadanoff-Baym contour.

The system of the equations (9)–(12) can be solved by iteration starting from some initial guess for the self-energy $\Sigma^c(t, t')$. From Eq. (9), one can find the local Green's function $g^{c-1}(t, t')$, which allows us to find the effective dynamical mean field $\lambda^c(t, t')$ from Eq. (10). Then the impurity equation [Eq. (11)] allows us to find a new local Green's function, which is employed to find a new self-energy from Eq. (12). This procedure is repeated until the self-energy has converged to a fixed point. We call this iterative solution approach the DMFT algorithm.

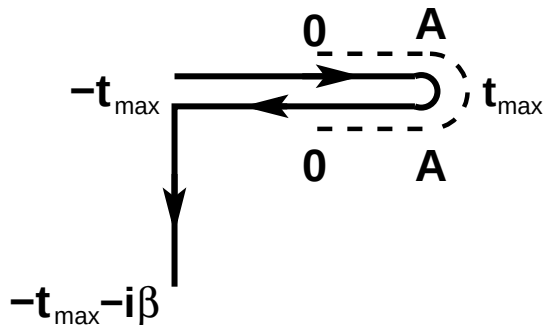

Fig. 1. Kadanoff-Baym integration contour for the time variables. The time-domain cutoffs are symmetric at $\pm t_{\max}$. The direction for the integration of the line integral is indicated by the arrows. The dashed line schematically shows where we typically turn on the electric field, as represented by the vector potential; it is commonly turned on when the time is equal to zero. Note that for the lesser functions, we choose the first time argument on the upper real time branch, and the second time argument on the lower real branch. When the contour is discretized, we use a step spacing of Δt along the real axis, and a step size of 0.05 along the imaginary axis. All calculations presented here have $\beta = 1$ corresponding to twenty steps along the imaginary axis.

Once the system of equations in Eqs. (9)–(12) is solved, then we can determine the properties of the system as a function of time. It is convenient to describe response functions like the self-energy and the Green's function with the relative $t_{\rm rel}$ and the average T time variables (the so-called Wigner coordinates [12]):

$$t_{\rm rel} = t - t', \quad T = \frac{t + t'}{2}, \tag{13}$$

instead of the two times t and t'. In equilibrium, these functions are independent of the average time T, and depend only on the relative time $t_{\rm rel}$. We perform a Fourier transform of the relative time to a real frequency, and examine the Green's function and self-energy as functions of frequency. In the nonequilibrium case, we do a similar thing, performing the Fourier transform with respect to the relative time, and examining how the response functions evolve as a function of the average time. For example, we have

$$\Sigma^<(\omega, T) = \int dt_{\rm rel} e^{i\omega t_{\rm rel}} \Sigma^c \left(T + \frac{t_{\rm rel}}{2}, T - \frac{t_{\rm rel}}{2} \right). \tag{14}$$

Note that we must have the first time argument $t = T + t_{\rm rel}/2$ lying on the upper branch and the second time argument $t' = T - t_{\rm rel}/2$ lying on the lower branch of the Kadanoff-Baym contour.

Another interesting quantity is the current density that is driven by the external electric field:

$$\mathbf{j}_l(T) = -i \frac{et^*}{\sqrt{d}} \sum_{\mathbf{k}} \sin \left(\mathbf{k}_l - \frac{e\mathbf{A}_l(T)}{\hbar c} \right) g^<(\varepsilon_{\mathbf{k}}, \bar{\varepsilon}_{\mathbf{k}}, T, T), \tag{15}$$

with each vector component identical when the electric field lies along the diagonal. The magnitude of the total current density in the case where the electric field lies along the unit-cell diagonal is then

$$j(T) = \sqrt{d} \mathbf{j}_l(T). \tag{16}$$

It is well known that the current response to an electric field is strange for a perfect conductor that has no electron scattering. Indeed, there is an ac response to a dc field due to the lattice periodicity, which does not allow the momentum of the electron to get too large before an umklapp scattering event occurs with the lattice and changes the sign of the momentum. This phenomenon is called a Bloch oscillation [13], [14], [15], and it should be seen in any material that is free enough of defects and other sources of scattering. No conventional metal has ever been grown that has small enough scattering to exhibit Bloch oscillations. Instead, the scattering occurs so rapidly, that the steady-state current is a constant, which increases linearly with the electric field until nonlinear effects take over. Bloch oscillations have been seen in semiconducting heterostructures [16]

Bloch oscillations are also seen in DMFT, with a time-independent electric field (E constant and $A(T) = -EcT$) [8]:

$$j(T) \sim \sin \left(\frac{eA(T)}{\hbar c} \right) \int d\varepsilon \frac{df(\varepsilon - \mu)}{d\varepsilon} \rho(\varepsilon), \tag{17}$$

producing an oscillating current density [$\rho(\varepsilon)$ is the noninteracting density of states, which is equal to the integral of ρ_2 over $\bar{\varepsilon}$ and $f(\varepsilon) = 1/\{1 + \exp(\beta\varepsilon)\}$ is the Fermi-Dirac distribution]. The frequency of the oscillation is $\omega_{\rm Bloch} = eE/\hbar$ and is called the Bloch oscillation frequency. We expect these oscillations to survive in the presence of scattering if the field is large enough that the relaxation time due to scattering is significantly larger than the Bloch oscillation period. The frequency of oscillation is undoubtedly too high for the Bloch oscillations to be directly observed ($\omega_{\rm Bloch} \gg 10^{12}$ Hz).

III. Numerical algorithm

There are a significant number of numerical issues that need to be taken into account to be able to determine the Green's functions, and other properties of strongly correlated electrons

in a large electric field. To begin, the matrix operators are continuous operators defined along the Kadanoff-Baym contour, and there is no simple way to find their matrix inverse analytically. Furthermore, matrix multiplication implies an integration over the Kadanoff-Baym contour

$$A \cdot B(t,t') = \int_c dt'' A(t,t'')B(t'',t'), \tag{18}$$

which is a complicated line integral in the complex plane (see Fig. 1). Our approach to solve this problem is a common numerical approach—we discretize the Kadanoff-Baym contour and evaluate the line integrals as finite Riemann sums over the discretized paths. The matrix operators then become finite-dimensional square matrices, whose size is equal to the number of points used to discretize the Kadanoff-Baym contour. Once this has been accomplished, then standard LAPACK and BLAS routines can be employed to invert and manipulate the discretized versions of the matrix operators. One issue that needs to be taken into account though is that the inverse of a continuous matrix operator satisfies

$$\int_c dt'' A^{-1}(t,t'')A(t'',t) = \delta_c(t,t') \tag{19}$$

with δ_c the Dirac delta function on the contour. The delta function is represented by the inverse of the time step used in the discretization of the Kadanoff-Baym contour, but one needs to note that this time step changes sign on the lower (real) branch of the contour, and it becomes imaginary on the vertical piece of the contour. One needs to properly take this into account before using a matrix inversion routine.

Next, we need to examine the numerical issues arising in Eq. (9). We evaluate this equation for a given self-energy matrix $\Sigma^c(t,t')$. This requires us to choose values of ε and $\bar{\varepsilon}$ for the two-dimensional Gaussian integration, compute the inverse of the matrix $g_0^c(\varepsilon,\bar{\varepsilon})$, subtract the self-energy, and compute a new matrix inverse. There is an exact algorithm that allows us to directly compute the matrix inverse of $g_0^c(\varepsilon,\bar{\varepsilon})$; this arises from the equation of motion for the Green's function, from which the inverse operator can be directly read off. The only subtlety is to ensure that the inverse operator inherits the correct boundary condition from the Green's function. This is not so simple to carry out, but using techniques like the discretization scheme in Negele and Orland [17] and Kamenev [18] provides a systematic method to directly compute the matrix inverse which satisfies the requisite boundary condition and becomes the exact matrix-operator inverse in the limit where the discretization step size goes to zero. The last matrix inversion is a general complex matrix inversion, because the self-energy is complex-valued, and has no simple symmetries. Hence, it is the most "expensive" matrix inversion that needs to be performed. Next the matrix elements of the inverse are multiplied by the relevant weighting factors for the integration, and finally we accumulate the results over all ε and $\bar{\varepsilon}$ terms that we choose for the two-dimensional integral. Since the integral weights are Gaussian, it seems reasonable to employ a Gaussian integral scheme for choosing the points on the grids and the weights. Unfortunately, since each point in the two-dimensional integration requires one full matrix inversion, we need to minimize the number of points chosen. As a compromise, we use the following scheme: (i) we perform the integral using an $N = 54$ Gaussian integration; (ii) repeat with an $N = 55$ Gaussian integration; and (iii) average the results. The $N = 54$ case requires 2916 grid points and the $N = 55$ case requires 3025 grid points. We choose to average these two results, because terms in the Green's function often behave like $\exp(ic\varepsilon)$, which can be accurately represented by the Gaussian integration until c becomes on the order of the inverse of the grid spacing of the Gaussian integration near $\varepsilon = 0$. Then, the sampling over the discrete points will no longer cancel, and the Gaussian integration will overestimate the value of the integral. Since the grid spacing for $N + 1$ points nearly interlaces that for N, the results of the averaging over N and $N + 1$ grids produces accurate results for values of c up to two times larger than what is possible for either one alone, and in the double integral case, it produces a factor of two reduction in computation time from using a Gaussian integration scheme with twice the number of points.

This part of the DMFT algorithm, the calculation of the local Green's function from the self-energy, is easily parallelized. One simply ships the self-energy matrix, and the energy variables ε and $\bar{\varepsilon}$ to the individual nodes, generates the relevant matrix, performs the inversion, and sends the result back to the master node for accumulation. Once the local Green's function has been calculated, then we proceed with the remainder of the DMFT algorithm to determine the new self-energy matrix. This part of the code is not so simple to parallelize, because it must proceed in a serial fashion. The only possible parallelization will occur if we can use SLAPACK routines to distribute the calculation of the matrix inverses over a small set of processors. To date, we have not included this element in the computation.

The algorithm given by Eqs. (9)–(12) is iterated until it converges. As the size of the matrices is made larger, by choosing a larger maximal cutoff in time for the Kadanoff-Baym contour, or by fixing the maximal cutoff time and reducing the step size, then the algorithm slows down significantly, and it becomes more difficult to attain the same level of accuracy at the end of the iterations. We usually try to iterate the solutions at least $20 - 50$ times for full convergence, but sometimes we have to limit ourselves to about 10 iterations due to the computational time involved.

There are a number of numerical issues that play a role in the quantitative accuracy of the results. These include the maximal time chosen for the cutoff $t_{\max}$, the step size in real time Δt, and the number of points N chosen for the ε grids. In this work, we examine a number of different choices for these parameters to see which terms are the most important for maintaining accuracy of the results. We do this employing what is probably one of the most difficult cases for the nonequilibrium code, that of a vanishing electric field (corresponding to an equilibrium situation). There is a major simplification of this approach because we have no $\bar{\varepsilon}$ dependence in our formulas, and the integral over $\bar{\varepsilon}$ can be done trivially. The problem arises from the fact that the self-energy develops a delta function in frequency at $\omega = 0$ in the insulating state, and this function cannot be easily represented in a calculation for real time that has a finite cutoff along the time axis. Indeed, we find that it is difficult

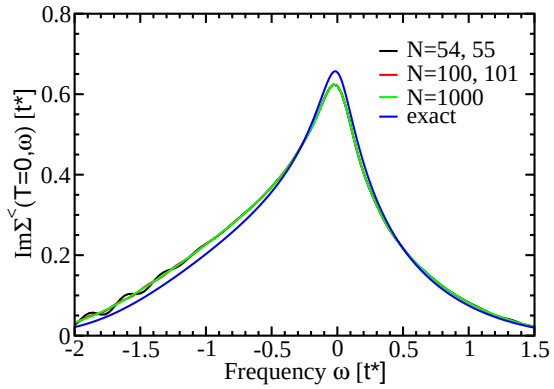

Fig. 2. Lesser self-energy for $\beta = 1$, $U = 1$, and half-filling. We examine the frequency dependence of the self-energy at an average time $T = 0$ and in equilibrium, but calculated with the nonequilibrium formalism. The exact results are in blue, and the other curves are all calculated with $\Delta t = 0.05$ and $t_{\max} = 15$. The black curve uses Gaussian integration with $N = 54$ and 55 points. The red curve is for $N = 100$ and 101 points, and the green curve is a trapezoidal rule with 1000 points evenly spaced between -3 and 3.

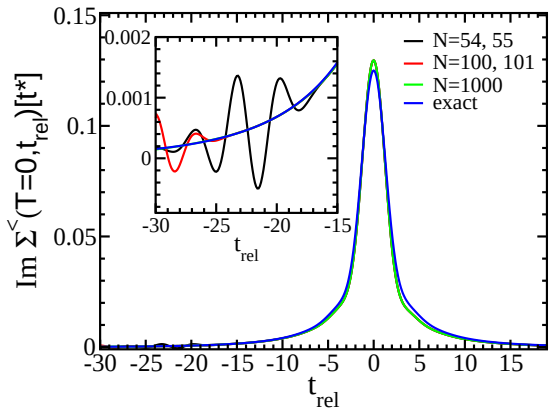

Fig. 3. Imaginary part of the lesser self-energy for $\beta = 1$, $U = 1$, and half-filling. We examine the relative time dependence of the self-energy at an average time $T = 0$ and in equilibrium, but calculated with the nonequilibrium formalism. The exact results are in blue, and the other curves are all calculated with $\Delta t = 0.05$ and $t_{\max} = 15$. The colors of the other curves are identical to those in Fig. 2. Inset is a blow up of the region around $t_{\rm rel} = -20$, where the integration over ε introduces spurious results when the grid spacing is too coarse, which lead to the oscillations seen in Fig. 2.

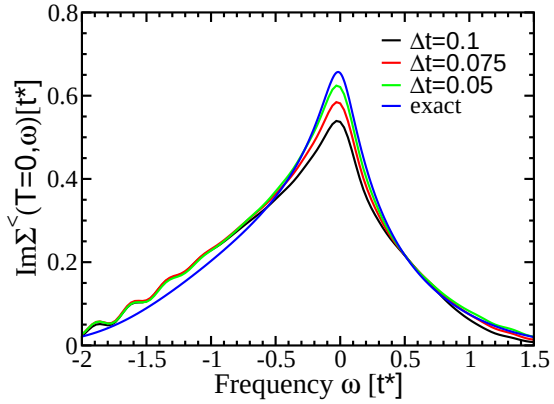

Fig. 4. Lesser self-energy for $\beta = 1$, $U = 1$, and half-filling for different discretizations of the Kadanoff-Baym contour. The exact results are in blue, and the other curves are all calculated with $N = 54$ and 55 points for the Gaussian integration and $t_{\max} = 15$. The black curve has $\Delta t = 0.1$. The red curve has $\Delta t = 0.075$ and the green curve has $\Delta t = 0.05$.

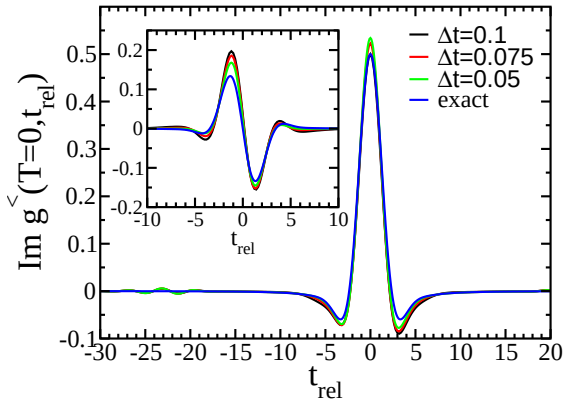

Fig. 5. Lesser Green's function for $\beta = 1$, $U = 1$, and half-filling for different discretizations of the Kadanoff-Baym contour. We plot the results for $T = 0$ as a function of $t_{\rm rel}$. The main panel is the imaginary part, and the inset is the real part. The exact results are in blue, and the other curves are all calculated with $N = 54$ and 55 points for the Gaussian integration and $t_{\max} = 15$. The black curve has $\Delta t = 0.1$. The red curve has $\Delta t = 0.075$ and the green curve has $\Delta t = 0.05$. Note that the exact result is an even function of $t_{\rm rel}$ for the imaginary part and an odd function for the real part.

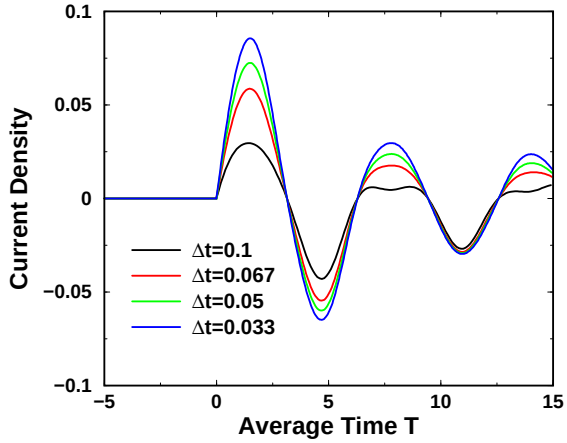

Fig. 6. Current density as a function of time for $U = 0.5$ and various values of Δt ($t_{\max} = 15$ and $N = 54$, 55 Gaussian integration). The temperature is fixed at $\beta = 1$ and the electric field satisfies $E = 1$. Note how the current converges to a "fixed point" as $\Delta t \to 0$, but not uniformly.

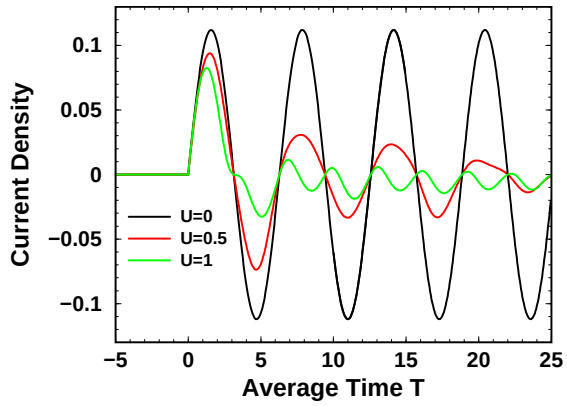

Fig. 7. Current density as a function of time for $U = 0$, 0.5, and 1. The temperature is fixed at $\beta = 1$ and the electric field satisfies $E = 1$ ($N = 54$, 55 Gaussian integration). Note how the Bloch oscillations are damped as the scattering increases, and how the period might be modified.

to obtain good results for the self-energy as a function of frequency in this case. But we also check the moments of the self-energy and the Green's function, and find good agreement for the low-power moments, indicating that the results do work well for short times. Hence, it is reasonable to think that they do a good job at determining the initial transient response to an electric field after the field is turned on. Furthermore, we do not know whether the delta function in the self-energy survives when a field is turned on. If it doesn't, then the nonequilibrium approach may work well for the insulating cases, even if it has problems for the equilibrium system.

IV. Benchmarking the equilibrium results

The electronic density of states is a quantum-mechanical measure of the elementary excitations of a strongly correlated material. In most materials, the density of states spans a range of a few electron volts, or in our units, a few t^*. The Fourier transform of the density of states is closely related to the Green's functions in the time domain. We expect the time-dependent Green's functions to have important time dependence when $t_{\rm rel}$ is smaller than c/t^* for some constant c of order one. Hence choosing a cutoff in time on the order of $10 - 20\ 1/t^*$ is a reasonable choice. The above heuristic discussion holds when the system is metallic. When it becomes insulating, then the density of states has a gap, and the self-energy develops a pole, for small frequencies. In this case, we need a large time domain (infinite in the case of a delta function) to properly reproduce the density of states or self-energy after Fourier transforming. This means that the time-domain cutoff needs to be made larger as the electron correlations are made stronger.

Similarly, the more fine-structure that is present in the Green's functions as functions of time, the smaller the step size Δt in the time domain needs to be to be able to accurately discretize the matrix operators. In general, we expect the discretization error to grow as the electron correlations increase, so Δt will need to be reduced for larger values of U. We typically choose $\Delta t = 0.1 - 0.05$ in our calculations. Obviously, we cannot keep increasing the time domain, and decreasing the step size when we have finite computational resources. The maximal matrix that we consider has a size on the order of 2500×2500. This choice is not a function of memory limitations, but rather is an issue of the computational time needed to invert these matrices as part of the DMFT algorithm. The bottom line is that these calculations will not be able to be pushed to too large a value for U without running into resource problems.

In order to benchmark our code, we have chosen to examine the equilibrium solutions using the nonequilibrium formalism. This is a particularly nice exercise to undertake, because the equilibrium solutions are all known to high accuracy via a direct solution using an algorithm in the frequency domain [10], [11]. It is also a challenging test of the nonequilibrium codes, because we need to Fourier transform the solutions in time to functions of frequency, and the effects of the discretization step size, and of the time-domain cutoff can play critical roles in the accuracy. The other important parameter in governing the accuracy is the step size employed in the energy integrations to determine the local Green's function. As discussed above, if the step size is too large, then we can generate spurious signal at large relative times, which will Fourier transform into high-frequency wiggles in the frequency domain. If we know that such structures are not present in the exact results, we can easily filter them out, but this becomes problematic when we are not sure whether such structures are real or numerical artifacts (which occurs when we perform nonequilibrium calculations).

We benchmark our results by examining the equilibrium solutions at high temperature ($\beta = 1$) and for a large value of U ($U = 1$) that is still in the metallic phase (the metal-insulator transition occurs at $U = \sqrt{2}$). We choose this for our initial benchmarking exercise because the self-energy does not have a pole; hence, the numerical issues should be under better control. We will briefly discuss issues that occur in the insulating phase below.

Our first result is shown in Fig. 2. It plots the lesser self-energy at $T = 0$ as a function of ω, which is calculated by performing the Fourier transformation with respect to $t_{\rm rel}$. This result should be independent of T, because we are in equilibrium, but the results do have a small dependence on T, that is due to the fact that we have instituted a finite cutoff in time $t_{\rm max} = 15$. In this figure, we study how sensitive the results are to changing the number of points in the integration over ε (recall, the integration over $\bar{\varepsilon}$ is trivial when we are in equilibrium). The blue curve is the exact result, the black curve employs Gaussian integration, averaging over the $N = 54$ and $N = 55$ cases, while the red curve is similar with $N = 100$ and $N = 101$ points. The green curve uses a much smaller step size in ε, employing $N = 1000$ points in a trapezoidal rule integration, ranging from -3 to 3. Note how all of the results lie on top of each other for small ω, although they do differ from the exact result. In the tails, for larger $|\omega|$, we see oscillations develop for the Gaussian integrations, that are reduced as the step size is made smaller, and completely disappear by the time $N = 1000$. These results show that by carefully controlling the step size used for the energy integration, one can obtain converged results without any extraneous oscillations, but those converged results are not exact, because they were calculated with finite values for Δt and $t_{\rm max}$.

In Fig. 3, we show the results for the imaginary part of the lesser self-energy as a function of $t_{\rm rel}$. Once can see particularly good quantitative agreement for small times, and then there is a region with oscillations out in the tail ($t_{\rm rel} \approx -20$). This region is blown up in the inset. The oscillations are only present for the coarse ε integrations, and the amplitude of the oscillations shrinks as the step size is made smaller. It is precisely these spurious results that lead to the oscillations in the Fourier transform (see Fig. 2). If we know about this kind of spurious behavior, we can filter the oscillations out before performing the Fourier transform, but this is an *ad hoc* procedure that cannot be generalized to the nonequilibrium case.

In Fig. 4, we show the Δt dependence of the calculations with fixed values for $t_{\rm max} = 15$, and $N = 54$ and $N = 55$ averaged Gaussian integrations. The results vary the most at small frequency, and appear to systematically approach the exact result as $\Delta t \to 0$. The results are less sensitive to Δt for larger frequencies, and since we have already seen that reducing the

step size in ε tends to only smooth out the oscillations (without changing the shape too much), the errors at higher frequencies must be coming from the finite cutoff $t_{\max}$.

Finally, we show the Green's function as a function of $t_{\rm rel}$ in Fig. 5. The imaginary part is in the main plot, and the real part is in the inset. In the exact result (blue curve), the imaginary part is an even function, and the real part is an odd function. The results of the nonequilibrium calculation do not share this symmetry, but it appears to be getting restored as $\Delta t \to 0$. More problematic is the issue of the value of $g^<$ at $t_{\rm rel} = 0$, which is determined solely by the electron filling. The results appear to be getting worse as $\Delta t \to 0$. It must be that if we increase the time cutoff, the results will ultimately start moving back toward their correct value, but we cannot check this explicitly due to the finite computer resources that are available.

We can be more quantitative about the short time behavior though. To do so, we can calculate the first few moments of the integrals of the Green's function and the self-energy over ω, and compare them to the exact results for those integrals. The zeroth moment relates to the function at $t_{\rm rel} = 0$, the first power to the slope, and the second power to the curvature. When we examine the results for $U = 0.5$ and $U = 1$, we find the zeroth moment of g and Σ is in error by about 7%, the first moment by 10% for g and 20% for Σ, and the second moment of g and Σ by $15 - 20$%. The results do not depend too strongly on the step size for ε in the integrations, as expected, because the oscillations average out of the moments. The first moment appears to extrapolate to its correct value as $\Delta t \to 0$ for the $N = 54$, 55 Gaussian integration with a fixed $t_{\max}$, but the zeroth and second moments do not appear as if they scale to the right result. This is most likely due to the fact that the $t_{\max}$ needs to be increased, but the large step size for ε may also play a role.

When we try to examine the insulating phase, we find the agreement with the exact results becomes much worse. This is because there are low-energy features which require large times to be determined accurately. Also, the larger U, the smaller Δt needs to be to obtain good accuracy. Our results for $U = 1.5$ are too preliminary to report quantitative values here.

The important question is whether these low-energy features survive as the electric field is turned on. If they are destroyed by the field, then the computational scheme that we are using should be able to accurately determine nonequilibrium results at short times. If they survive, then it will be difficult to get high accuracy results for the nonequilibrium case in the Mott insulator. Since the presence of a field pumps energy into the system, and that energy can be used to create excitations across a gap, it is easy to believe that the gap features do not survive the introduction of a large electric field, but we cannot definitively say whether this is actually true at this point.

V. Bloch oscillations

One of the most interesting nonlinear phenomena of a material is the production of Bloch oscillations in the current as a function of time when a constant (dc) electric field is applied. In the absence of interactions (which cause scattering), the current will oscillate forever, with a constant amplitude (the period is determined by the strength of the electric field). As we turn on the scattering, we expect the oscillations to be dampened, but perhaps to maintain the same period (and even survive in the steady state). If the scattering becomes large enough, then the oscillations should disappear completely. By calculating the Green's functions in the presence of a field that is turned on at $T = 0$, we can study how the current initially starts, and how it evolves into a steady state. Due to the need for a finite $t_{\max}$, we can only go so far out in time before the calculation must terminate.

In Fig. 6, we plot the Bloch oscillations of the current as a function of the average time, for $U = 0.5$, $\beta = 1$, $E = 1$, and the $N = 54$, 55 Gaussian integration scheme. The $t_{\max}$ is equal to 15. As Δt is reduced, one can clearly see that the results are beginning to converge. Furthermore, it is also clear that there is a damping of the transient response as we move forward in time. We examine the behavior of this transient damping in Fig. 7, where we have preliminary results for the current density for three values of U. The results for $U = 0.5$ and $U = 1$, are calculated with a step size of $\Delta t = 0.05$. At the moment, it is not clear how much of an effect the boundaries at $t_{\max}$ have on the results, but it may be that the largest time results are not fully trustworthy. Some interesting behavior can be seen in the figure: (i) we see the damping that is expected, and that it gets more strongly damped as U is increased; (ii) as U is increased, it appears that the period may be decreasing, which is not an expected result; and (iii) the behavior of the transient evolution is quite complex, and we do not appear to have reached the steady state yet.

VI. Conclusions

In conclusion, we have shown that there is a straightforward way to perform many-body physics calculations in real time for both equilibrium and nonequilibrium situations by formulating the problem on a Kadanoff-Baym contour and discretizing it. There are a number of numerical issues that arise from this approach, coming from the discretization of the contour and its truncation, as well as from the discretization of the energy space needed to perform numerical quadratures. By using the equilibrium results as a benchmark, we can see how the different discretization operations affect the overall accuracy of the calculations. It seems like the small-time behavior can be understood fairly well by using reasonable choices for the discretizations and the time-domain cutoffs. It is more difficult to obtain good results for the longer-time behavior. One also needs to have good control of the numerics to be able to accurately perform Fourier transformations to real frequency. Maintaining control of these different approximations is made more difficult by the finite computational power that is available to solve these problems.

The fact that we must iterate our equations to a self-consistent solution brings a number of unknown issues to the table. First, we have modified the Green's function by introducing a time-domain cutoff, which is artificially changing the boundary conditions. It is well known that Green's functions are determined uniquely by their equation of motion and their boundary conditions. How much of an effect the change of the boundary condition has on the results is difficult to estimate because of the nonlinearities introduced by the iterative solution.

Second, we are not able to iterate the equations for an infinitely long period of time, so the smaller we make the discretizations, the fewer iterations we are able to complete. For example, when the matrices have a size on the order of 700×700, we can easily perform 50 or more iterations, but we are reduced to about 7 iterations when they are 2000×2000. It is difficult to tell how much error is introduced by this.

In the future, we will use this technique to study and analyze better the behavior of strongly correlated materials in a large electric field. Eventually, we hope to be able to generalize this approach to apply it to multilayered nanostructures and thereby be able to directly calculate the current-voltage characteristic of a strongly correlated device.

VII. Acknowledgments

We acknowledge support of the Office of Naval Research under grant number N00014-99-1-0328 and from the National Science Foundation under grant number DMR-0210717. Supercomputer resources (Cray T3E and X1) were provided by the Arctic Region Supercomputer Center (ARSC) and the Engineering Research and Development Center (ERDC).

References

[1] Kadanoff, L. P. and Baym, G., *Quantum Statistical Mechanics*, (W. A. Benjamin, Inc., New York, 1962).

[2] Keldysh, L.V., "Diagram Technique for Nonequilibrium Processes," *J. Exptl. Theoret. Phys.* **47**, 1515–1527, 1964 [*Sov. Phys. JETP* **20**, 1018–1026, 1965].

[3] Mukhanov, O.A., Semenov, V. K. and Likharev, K. K., "Ultimate performance of the RSFQ logic circuits," *IEEE Trans. Magn. Mater.* **MAG-23**, 759–762, 1987; Likharev, K. K., "Superconductor devices for ultrafast computing," in *Applications of Superconductivity* Ed. by Weinstock, H. (Kluwer, Dordrecht, 2000), Ch. 5.

[4] Falicov, L. M. and Kimball, J. C., "Simple model for semiconductor-metal transitions: SmB_6 and transition-metal oxides," *Phys. Rev. Lett.* **22**, 997–999, 1969.

[5] Peierls, R. E., "Theory of diamagnetism of conduction electrons", *Z. Phys.* **80**, 763–791, 1933.

[6] Jauho, A. P. and Wilkins J. W., "Theory of high-electric-field quantum transport for electron-resonant impurity systems," *Phys. Rev. B* **29**, 1919–1938, 1984.

[7] Metzner, W. and Vollhardt, D. "Correlated Lattice Fermions in $d = \infty$ Dimensions," *Phys. Rev. Lett.* **62**, 324–327, 1989.

[8] Turkowski, V. and Freericks, J. K., "Nonlinear response of Bloch electrons in infinite dimensions", *Phys. Rev. B* **71**, 085104-1–11, 2005.

[9] Schmidt, P., "Time-dependent dynamical mean-field theory", Diplome thesis, University of Bonn, 2002.

[10] Brandt, U. and Mielsch, C. "Thermodynamics and correlation functions of the Falicov-Kimball model in large dimensions," *Z. Phys. B–Condens. Mat.* **75**, 365–370, 1989; "Thermodynamics of the Falicov-Kimball model in large dimensions II," *Z. Phys. B–Condens. Mat.* **79**, 295–299, 1990.

[11] Freericks, J. K., and Zlatić, V., "Exact dynamical mean field theory of the Falicov-Kimball model," *Rev. Mod. Phys.* **75**, 1333–1382, 2003.

[12] Wigner, E., "On the quantum correction for thermodynamic equilibrium", *Phys. Rev.* **40**, 749–759, 1932.

[13] Bloch, F., "Quantum mechanics of electrons in crystals", *Z. Phys.*, **52**, 555–599, 1928.

[14] Zener, C., "A Theory of the Electrical Breakdown of Solid Dielectrics", *Proc. R. Soc. (London) Ser. A* **145**, 523-529, 1934.

[15] Aschcroft, N. W. and Mermin, N. D. *Solid State Physics*, (Holt, Rinehart, and Winston, Philadelphia, 1976).

[16] Waschke, C., Roskos, H. G., Schwedler, R., Leo, K., Kurz, H., and Köhler, K. "Coherent submillimeter-wave emission from Bloch oscillations in a semiconductor superlattice", *Phys. Rev. Lett.* **70**, 3319–3322 (1993).

[17] Negele, J. W. and Orland, H., *Quantum Many-Particle Systems* (Addison-Wesley Publishing Company, Redwood City, CA, 1988).

[18] Kamenev, A. "Keldysh and Doi-Peliti techniques for out-of-equilibrium systems," in *Strongly correlated fermions and bosons in low dimensional disordered systems*, NATO Science Series II: Mathematics, Physics and Chemistry, Vol. **72**, edited by Lerner, I. V., Altshuler, B. L., Fal'ko, V. I., and Giamarchi, T. (Kluwer, Dordrecht, 2002).